

Retrieval of Biomass in Boreal Forests from Multitemporal ERS-1 and JERS-1 SAR Images

Lauri Kurvonen, Jouni Pulliainen, and Martti Hallikainen, *Fellow, IEEE*

Abstract—The response of JERS-1 and ERS-1 synthetic aperture radar (SAR) to the forest stem volume (biomass) was investigated by employing a digital stem volume map and weather information. The stem volume map was produced from the National Forest Inventory sample plot data together with a LANDSAT thematic mapper (TM) image. A new indirect inversion method was developed and tested to estimate the forest blockwise stem volume from JERS-1 and/or ERS-1 SAR images. The method is based on using a semiempirical backscatter model for inversion. The model presumes that backscatter from a forest canopy is determined by the stem volume, soil moisture, and vegetation moisture. The area of interest is divided into a training and test area. In this study, the training area was 10% of the test site, while the remaining 90% was used for testing the method. The inversion algorithm is carried out in the following three steps.

- 1) For the training area, the soil and vegetation moisture parameters are estimated from the backscattering coefficients and stem volume (must be known for training areas) with the semiempirical backscatter model.
- 2) For the area of interest, the stem volume is estimated from the moisture parameters and backscattering coefficients with the semiempirical backscattering model.
- 3) If several SAR images are used, the stem volume estimates are combined with a multiple linear regression. The regression equation is defined using the stem volume estimates for the training area.

The results for the stem volume estimation using *L*-band and/or *C*-band SAR data showed promising accuracies: the relative retrieval rms error varied from 30 to 5% as the size of the forest area varied from 5 to 30 000 ha (the forest stem volume varied from 0 to 300 m³/ha).

Index Terms—Backscattering properties of boreal forests, ERS-1 synthetic aperture radar (SAR), forest biomass estimation, JERS-1 SAR.

I. INTRODUCTION

THE BOREAL forest belt covers large areas of Europe, Asia, and North America, forming the largest vegetation zone on earth. Coniferous trees, such as pines and spruces, are the dominating tree species in this biotype. A large seasonal temperature variation is typical for the area. Therefore, the growing season is halted for winter when the ground is frozen and covered by snow. Finland is located in the boreal forest belt, and its forests compose a spatially varying mosaic consisting of forest blocks that typically cover an area of a few hectares, on privately owned land about 1 ha. A forest

block is defined as a homogeneous forest unit in which tree-cover, treatment procedures, and site class (soil fertility class) are about the same. The availability of extensive ground truth information on large forest areas makes the Finnish forests favorable for remote-sensing research.

In our studies on boreal forests, inversion methods have been developed for both active and passive satellite-borne microwave sensors [1]–[4]. The objectives have been *biomass estimation, forest, and land-cover type recognition*. Active microwave sensors [e.g., synthetic aperture radar (SAR)] have a good spatial resolution, but their radiometric resolution is moderate because of the coherent measurement method. In contradiction to active sensors, radiometers have good radiometric accuracy and wide coverage, but the spatial resolution is moderate (tens of kilometers). Therefore, a radiometer could be used for global monitoring, while a SAR would provide more detailed local information [3]. This paper presents the analysis and results on the biomass estimation with ERS-1 and JERS-1 SAR images.

Direct application of the backscattering coefficient for biomass retrieval is limited by saturation [5]–[8]. The saturation level is dependent on seasonal and weather conditions, which suggests the use a multitemporal image set for the biomass retrieval. The saturation level of SAR response to biomass increases with decreasing frequency [5], [7]–[10]. The *P*-band would be the most promising for biomass measurements, but it is not available on satellite-borne sensors. The JERS-1 satellite carries an *L*-band HH-polarization SAR that is the most feasible satellite radar for forest biomass estimation [11], [12]. Several studies have shown that correlation between the *C*-band backscattering coefficient and the forest biomass is low or negligible [5], [7]–[10]. Nevertheless, encouraging results were achieved with an indirect retrieval approach using ERS-1 SAR images [1]. Therefore, a selected set of ERS-1 images is also used in this paper.

When satellite-borne SAR images are used for forest applications, extensive averaging is needed, due to the high level of speckle in the images. The averaging can be partly processed in the time domain if several images are used. Therefore, a set of SAR images provides more reliable results with a higher spatial resolution than a single SAR image. However, recent studies have shown that seasonal effects, such as soil and snow cover freezing/thawing, drastically change the level of backscatter up to about 3–4 dB at *C*-band and 5–7 dB at *L*-band [13]–[17]. Typically, the seasonal effects cause larger changes on backscatter than the variation of the biomass. Thus, a direct retrieval approach is not useful for

Manuscript received June 30, 1997; revised February 10, 1998. This work was supported in part by the European Commission, under a Research Fellow Grant for L. Kurvonen at the Joint Research Centre, Ispra, Italy.

The authors are with the Laboratory of Space Technology, University of Technology, 02150 Espoo, Finland (e-mail: kurvonen@avasun.hut.fi).

Publisher Item Identifier S 0196-2892(99)00035-2.

a multitemporal image set. The seasonal effects have to be removed with suitable modeling before the biomass can be successfully retrieved from a multitemporal image set.

II. TEST SITE AND DATA SET

A. Test Site and Ground Truth

The size of our test site is 1800 km², and it is located in southern Finland (center coordinates 60° 30' N; 25° 30' E). The area contains various land-use classes: forests, mires, fields, urban areas, and water areas. The forests are conifer-dominated mixed forests, and their age variation is relatively small due to the industrial use. The test site represents well the Scandinavian forests. The dominating species are Norway spruce (60%) and Scots pine (30%). The elevation variation in the test site variation is less than 100 m. The ground truth consists of a digital stem volume map, a forest block map, and meteorological data.

1) *Digital Stem Volume Map*: The digital stem volume map is produced from the National Forest Inventory sample plot data together with LANDSAT thematic mapper (TM) images. The resolution is 25 m. The ground reference sample plots cover the test site, as well as the whole country, in a regular pattern: the sample plot clusters (tracts) are situated in 7–8-km intervals throughout the country, and each tract is an L-shaped pattern (length of both parts 2050 m) containing 21 sample plots (200-m intervals), each sized 400 m² [19]. The sample plot data include about 130 different forest parameters, such as the stem volume, tree species, tree age, basal area, soil type and land fertility class, and land use category. The stem volume ground truth was obtained from the Finnish Forest Research Institute, which is responsible for the National Forest Inventory [19]. The reliability of the stem volume values provided by the digital forest map increases with increasing sample plot. At pixel level, the relative rms error is about 50%, at 10-ha level, it is 30–40%, and at 50-ha level, it is around 25%, respectively [26].

2) *Forest Block Map*: For the purposes of this study, a forest block map was produced from the stem volume map. First, the stem volumes were divided with a pipeline classification into eight stem volume categories. Second, forest blocks were formed from neighboring pixels that belong to the same stem volume category. Third, the stem volume for each block was retrieved from the original stem volume map. The total number of forest blocks is about 16000, and they have an average size of 4.5 ha with a standard deviation of 9.5 ha. Typically, the total stem volume per hectare of the blocks varies from 0 to 300 m³/ha. The block mean stem volume is 133 m³/ha with a standard deviation of 62 m³/ha. According to [18], the stem volume (in m³/ha) can be approximately converted into the total aboveground dry biomass of trees (in tons/ha) by multiplying the stem volume by 0.6.

3) *Meteorological Data*: Meteorological data were recorded daily at three locations around the test site (Helsinki, Vihti, and Lahti, all of which are in Finland). The meteorological data include air temperature (daily minimum, average, and maximum), humidity, wind speed, cloud condition, and

TABLE I
ENVIRONMENTAL CONDITIONS DURING ERS-1
AND JERS-1 SAR DATA ACQUISITION

Date of ERS-1 SAR image	Precipitation (mm) (three-day cumulative sum)	Mean air temperature (°C)	Snow water equivalent (mm)
4 Aug. 1993	0.0	17.3	No snow
2 Oct. 1993	0.0	2.9	No snow
13 Oct. 1993	25.1	8.9	No snow
6 Nov. 1993	0.0	-0.2	No snow
Date of JERS-1 SAR image			
23 May 1993	0.5	12.6	No snow
18 Dec 1994	0.7	-6.0	0-5 (dry snow)
15 Mar. 1995	0.0	-1.2	40-60 (refrozen snow)
30 Apr. 1995	7.0	1.1	No snow

precipitation. The daily precipitation information was also obtained for a higher resolution grid.

B. Spaceborne Data

A total of eight SAR images were used in this study. Four ERS-1 PRI images were selected from the 23 images available. The selection was based on our previous study on these SAR images [1]. The original ERS-1 images, delivered in PRI format, were rectified and geocoded with a digital elevation model (DEM) by the Technical Research Center of Finland (VTT). The algorithm corrects the errors caused by topography, but no radiometric corrections were made to the image [26]. The geocoded ERS-1 images had a pixel spacing of 25 m, and the effective amount of looks was around four. All available JERS-1 images, covering the test site, were acquired from NASDA. The JERS-1 images (level 2.1) had a pixel spacing of 12.5 m, and three looks were used in the SAR processing. Based on ground truth control points, the JERS-1 images were georectified with a first-order polynomial function, but no topographic nor radiometric corrections were made to the image. The SAR images and the environmental conditions during the SAR data acquisition are listed in Table I.

The intensity values of the SAR images were converted to backscattering coefficients. The conversion equation for ERS-1 PRI images is [20]

$$\sigma^o = 20 \lg(i/1000) + C_{cal} \text{ dB.} \quad (1)$$

For JERS-1 level 2.1 images [21]

$$\sigma^o = 20 \lg(i) - 68.5 \text{ dB} \quad (2)$$

where i is the intensity on the SAR image and C_{cal} is an image-dependent calibration factor. Our inversion method employs forest blockwise averages for the backscattering coefficients. The calculation of the mean backscattering coefficients and their standard deviations was based on the localization from the forest block map.

III. METHODOLOGY

A. Backscattering Model

The backscattering coefficient of forest land (σ^o) can be presented as

$$\sigma^o = \sigma_V^o + t^2 \sigma_g^o \quad (3)$$

where σ_V^o is the backscattering coefficient of the forest canopy, t is the forest canopy transmissivity, and σ_g^o is the backscattering coefficient of the ground (including the trunk-ground reflection and surface vegetation).

The stem volume (biomass) inversion method is based on a semiempirical model [23]. The model was developed by analyzing a large number of measurements recorded with a high-resolution ranging scatterometer (HUTSCAT) that operates at C - and X -band [10], [23], [24]. When a forest is measured by a high-resolution ranging scatterometer, the two backscattering components in (3) can be separated. Moreover, the canopy transmissivity as a function of the forest stem volume can be determined by comparing $t^2 \cdot \sigma_g^o$ (the ground backscattering component) from areas with varying stem volumes. The analyses, discussed in [10] and [23], show that the backscattering coefficient in boreal forests is dominated by the stem volume, soil moisture, and vegetation moisture. Therefore, (3) can be written as [1], [10]

$$\sigma^o = \frac{C_1}{-2C_2} (1 - e^{2C_2 V}) + C_3 e^{2C_2 V} \quad (4)$$

where the first part of (4) represents the backscattering component of the forest canopy and the second part of (4) is the ground backscattering component. V is the stem volume, the parameters C_1 and C_2 are related to the vegetation moisture, and C_3 represents the backscatter from the ground. Using the cloud model [25], C_1 and C_2 can be presented as

$$C_1 = k_1 m_v^2 \quad (5)$$

$$C_2 = k_2 m_v \quad (6)$$

where m_v is the vegetation moisture and k_1 and k_2 are scaling factors. Previously, when the model was used for biomass retrieval at C -band [1], the scaling factors were defined from HUTSCAT measurements. Unfortunately, there are no suitable scatterometer measurements available at L -band. Therefore, in this study, the model is employed with parameters C_1 , C_2 , and C_3 and not with vegetation and soil moisture directly.

B. Inversion Algorithm

The inversion algorithm calculates an estimate for the forest blockwise stem volume from JERS-1 and/or ERS-1 SAR images. The algorithm uses a part of the data for training purposes. Therefore, the test site was divided for a training area (10%) and test area (90%). The forest blocks of the training set were spread uniformly on the test site, and the remaining forest blocks were used for testing the algorithm. In practice, the inversion algorithm has three steps and they are carried out as follows.

First Step: The parameters C_1 , C_2 , and C_3 of (4) are determined separately for each SAR image by employing (4) simultaneously for all training forest blocks. The set of equations is solved with the least-squares method with respect to C_1 , C_2 , and C_3

$$\sum_{i=1}^N (\sigma_{i, \text{EXP}}^o - \sigma_{i, \text{MODEL}}^o(V, C_1, C_2, C_3))^2 = \text{minimum} \quad (7)$$

where N is the number of training forest blocks, $\sigma_{i, \text{EXP}}^o$ is the measured mean backscatter for forest block i , and $\sigma_{i, \text{MODEL}}^o(V, C_1, C_2, C_3)$ is the modeled backscatter for forest block i .

Additionally, the training areas were divided into local subgroups and (7) was separately solved for each subgroup. These local scaling parameters were interpolated (bilinear) to cover the whole area of interest. This procedure was made to define the areal variation in the scaling parameters and its influence on the retrieval accuracy. Nevertheless, the global scaling factors provided significantly higher accuracies than the local scaling factors. Therefore, the results based on the global scaling factors are only presented and discussed in this paper.

Second Step: For the whole test site, the stem volume estimate for a forest block j is calculated from the measured blockwise mean backscattering coefficient (σ_j^o) and scaling factors C_1 , C_2 , and C_3 , by solving (4) with respect to the stem volume (V_j)

$$V_j = \frac{1}{2C_2} \ln \left(\frac{\sigma_j^o + \frac{C_1}{2C_2}}{C_3 + \frac{C_1}{2C_2}} \right) \quad (8)$$

The second step is carried out separately for each SAR image that is used in the retrieval process.

Third Step: If several SAR images are used in the process, the stem volume estimation from these images is combined with a multiple linear regression. The regression equation is defined from the stem volume estimate of the training areas and ground truth by solving

$$\sum_{i=1}^N (V_i - (\bar{L}_1 \bar{V}_{i, \text{EST}} + L_2))^2 = \text{minimum} \quad (9)$$

with respect to \bar{L}_1 and L_2 . In (9), N is the number of training forest blocks, V_i is the ground truth stem volume for a training forest block i , $\bar{V}_{i, \text{EST}}$ is a $(1 \times k)$ vector that has the stem volume estimates for the training forest block i based on the used k SAR images (see second step), \bar{L}_1 is a $(k \times 1)$ vector that has the regression coefficients, and L_2 is the regression bias (a scalar). Finally, the combined (final) stem volume estimation for a forest block j is calculated from $\bar{V}_{j, \text{EST}}$ (see second step), \bar{L}_1 , and L_2

$$V_{j, \text{COMBINED}} = \bar{L}_1 \bar{V}_{j, \text{EST}} + L_2 \quad (10)$$

TABLE II

ERS-1 AND JERS-1 SAR-BASED STEM VOLUME ESTIMATION FOR FOREST BLOCKS THAT ARE LARGER THAN 10 ha. THE CORRELATION IS CALCULATED BETWEEN THE ESTIMATED AND GROUND TRUTH STEM VOLUME. THE DYNAMIC RANGE AND SATURATION LEVEL ARE BASED ON THE VALUES PRESENTED IN FIGS. 1 AND 2. SCALING FACTORS ARE CALCULATED ACCORDING TO (7)

Date of SAR image	Dynamic range (dB)	Saturation level (m ³ /ha)	Scaling factors		
			C ₁	C ₂	C ₃
4 Aug. 1993	0.42	175	0.211×10^{-2}	-0.599×10^2	0.238
2 Oct. 1993	0.41	175	0.154×10^{-2}	-0.511×10^2	0.995×10^1
13 Oct. 1993	0.67	-	0.409×10^{-2}	-0.120×10^1	0.220
6 Nov. 1993	0.54	125	0.826×10^{-3}	-0.251×10^2	0.921×10^1
Date of JERS-1 SAR image					
23 May 1993	2.1	225	0.186×10^{-2}	-0.454×10^2	0.630×10^1
18 Dec. 1994	1.4	-	-0.439×10^{-3}	-0.106×10^2	0.573×10^1
15 Mar. 1995	1.6	-	-0.608×10^{-4}	0.123×10^2	0.8531×10^1
30 Apr. 1995	1.5	225	0.156×10^{-2}	-0.350×10^2	0.735×10^1

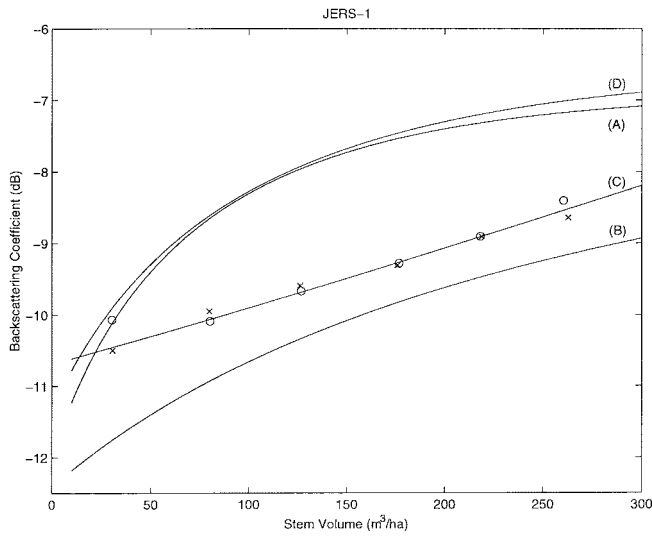


Fig. 1. Inversion function (8) employing the scaling factors based on JERS-1 images (see Table II). The curve (A) is for the JERS-1 image on May 23, 1993, (B) is for December 18, 1994, (C) is for March 15, 1995, and (D) is for April 30, 1995. As an example, the mean backscattering coefficients of the training and test set are presented for March 15, 1995. The training set is marked with "o," and the test set is marked with "x."

IV. RESULTS AND DISCUSSION

Every tenth forest block (without *a priori* information) was selected to the training set, and the numeral values for the scaling parameters (C_1 , C_2 , and C_3) were calculated according to (7). Table II shows the scaling parameters (the model fit) that were calculated in the first step of the inversion. These scaling parameters determine the shape of the inversion (8). Figs. 1 and 2 show the model fit function for the training set data of each employed SAR image. As an example, for one JERS-1 and ERS-1 image, the mean σ^o of the training set is marked with "o" and that of the test set is marked with "x" (with each SAR image, the mean σ^o matched well with the fit function). The level of the backscatter changed within 2 dB both in *C*-band (ERS-1) and *L*-band (JERS-1), depending on environmental conditions. For all JERS-1 SAR (*L*-band) images, the backscatter level increases with increasing stem volume, while for the ERS-1 (*C*-band)

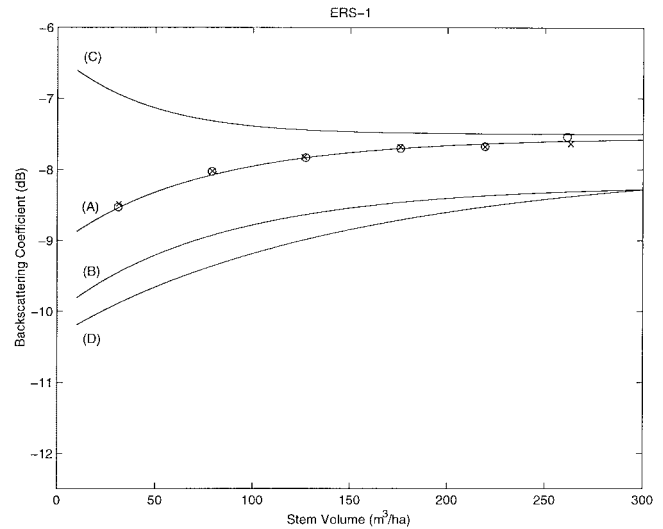


Fig. 2. Inversion function (8) employing the scaling factors based on ERS-1 images (see Table II). The curve (A) is for the ERS-1 image on August 4, 1993, (B) is for October 2, 1993, (C) is for October 13, 1993, and (D) is for November 6, 1993. As an example, the mean backscattering coefficients of the training and test set are presented for August 4, 1993. The training set is marked with "o" and the test set is marked with "x."

images, the relation between the backscatter and the stem volume is not straightforward. In the ERS-1 image for October 13, 1993, the wet ground was the dominating component in the backscatter; therefore, the backscatter level decreased with increasing stem volume. Table II shows the dynamic range of the backscatter with respect to the stem volume. The dynamic ranges are based on the mean backscattering coefficients of the six stem volume classes that are used in Figs. 1 and 2. For the ERS-1 images, the dynamic range was from 0.4 to 0.67 dB, while that for the JERS-1 images was from 1.4 to 2.1 dB. The saturation level in Table II is the stem volume class that had the highest mean backscattering coefficient (if it was not the highest stem volume class). Information in Figs. 1 and 2 and in Table II shows clearly that *L*-band (JERS-1) is more sensitive to the stem volume and less sensitive to environmental conditions than *C*-band (ERS-1).

The stem volume estimates for the forest blocks were calculated from each SAR image according to (8). Table III shows the results when forest blockwise stem volume was retrieved from a single SAR image. The inversion results are shown for forest blocks that are larger than 10 ha. The JERS-1 images for December 18, 1994, and March 15, 1995, provided the best results; the former had the lowest relative rms error (34%), while the latter had the highest correlation (0.65) between the estimated stem volume and the ground truth. Table II shows that for these two JERS-1 images the relation between the backscattering coefficient and the stem volume did not saturate. The ERS-1 image for November 6, 1993, provided the best result among the ERS-1 images, the correlation coefficient was 0.47, and the relative rms error was 49.6%. This image had the largest dynamic range of the ERS-1 images, when the image for October 13, 1993, was excluded (see Table II).

The stem volume estimation is strongly handicapped by the speckle when a single SAR image is used. When a relatively large area is considered, the speckle-based error can

TABLE III

ERS-1 AND JERS-1 SAR-BASED STEM VOLUME ESTIMATION FOR FOREST BLOCKS LARGER THAN 10 ha. THE STEM VOLUME ESTIMATION IS CALCULATED ACCORDING TO (8). THE CORRELATION IS CALCULATED BETWEEN THE ESTIMATED STEM VOLUME AND THE GROUND REFERENCE

Date of ERS-1 SAR image	Correlation coefficient r	Rms error of estimation (m ³ /ha)	Relative rms error of estimation (%)	Estimated mean stem volume of forest block (m ³ /ha)	Ground-truth mean stem volume of forest block (m ³ /ha)	Number of forest blocks
4 Aug. 1993	0.40	91.0	57.6	153	158	1233
2 Oct. 1993	0.41	92.7	58.7	154	158	1233
13 Oct. 1993	0.09	114	77.1	247	158	1233
6 Nov. 1993	0.47	78.3	49.6	162	158	1233
Date of JERS-1 SAR image						
23 May 1993	0.52	94.0	60.6	163	155	615
18 Dec. 1994	0.57	53.0	34.3	152	155	1351
15 Mar. 1995	0.65	56.3	36.8	161	153	320
30 Apr. 1995	0.53	71.7	46.6	169	154	414

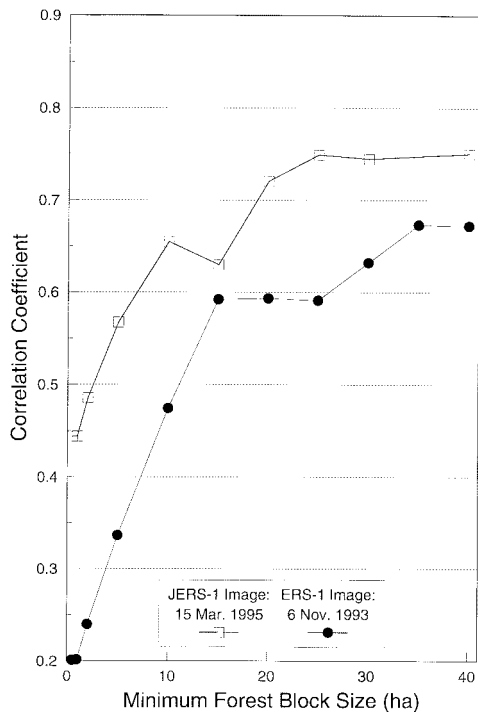


Fig. 3. Correlation coefficient r between the estimated stem volume and the ground truth versus minimum forest block size. The estimations are based on the JERS-1 image for March 15, 1995, and the ERS-1 image for November 6, 1993. The stem volume estimation is calculated according to (8).

be interpreted as normally distributed noise that has zero mean. Therefore, the spatial averaging reduces effectively the error in the inversion, and the forest block size is the dominating factor for the accuracy of the inversion process. Figs. 3 and 4 show the inversion results of the JERS-1 image for March 15, 1995, and the ERS-1 image for November 6, 1993, as a function of minimum forest block size. First, the rms error decreases rapidly with increasing minimum forest block size, but above the minimum size of 10–15 ha, the decline is relatively small. The correlation between the estimated stem volume and the ground truth saturates when the minimum size is from 20–30 ha. Figs. 3 and 4 show that the inversion method achieved

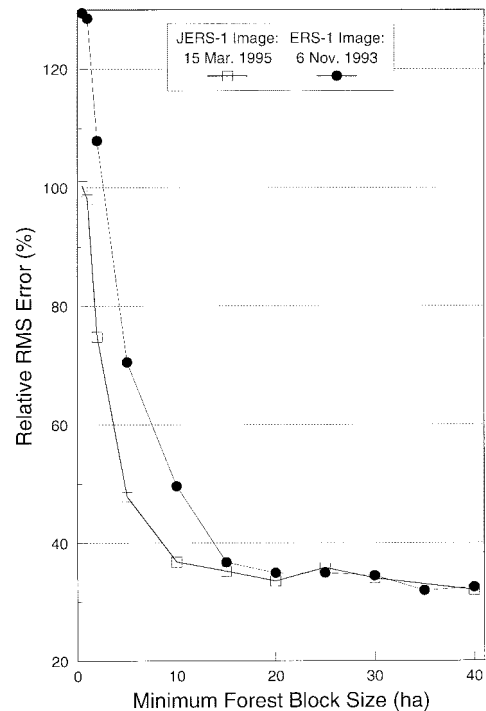


Fig. 4. Relative rms error of the stem volume estimations versus minimum forest block size. The estimations are based on the JERS-1 image for March 15, 1995, and the ERS-1 image for November 6, 1993.

relative accuracies of 30–40% with a single spaceborne SAR (JERS-1 or ERS-1) image. This rapid improvement in the accuracy was achieved by dismissing the small forest blocks, which are highly corrupted by speckle. For large-scale estimation, the results were even better. Table III presents the estimated mean stem volume for the forest blocks and the ground truth reference value. In most cases, the difference between the estimate and the reference value is from 3 to 10%.

The use of several images in the inversion process improves the accuracy of the method. The stem volume estimates based on different SAR images are combined with weighted averaging. The weights are based on the information value of the stem volume estimations. The weights were calculated with a multiple linear regression between the stem volume estimations and ground truth of the training areas according to (9). The weighting process ensures that a less informative image will not corrupt the information from a more informative image. Figs. 5 and 6 show the inversion result for a pair of JERS-1 and ERS-1 images. These pairs produced the best inversion results when a combination of two JERS-1 or ERS-1 images was used. When Figs. 5 and 6 are compared with Figs. 3 and 4, it is obvious that the accuracy improvement decreases with the increasing minimum forest block size. For a 0.5-ha minimum block size, the improvement was 50% for the JERS-1 image pair and 70% for the ERS-1 image pair, while at 10 ha, the improvement was 5% for the JERS-1 pair and 13% for the ERS-1 pair.

Figs. 7 and 8 show the inversion results when one to six SAR images are used in the inversion. Fig. 7 shows the correlation between the estimated stem volume and ground truth versus SAR image combination for forest blocks larger

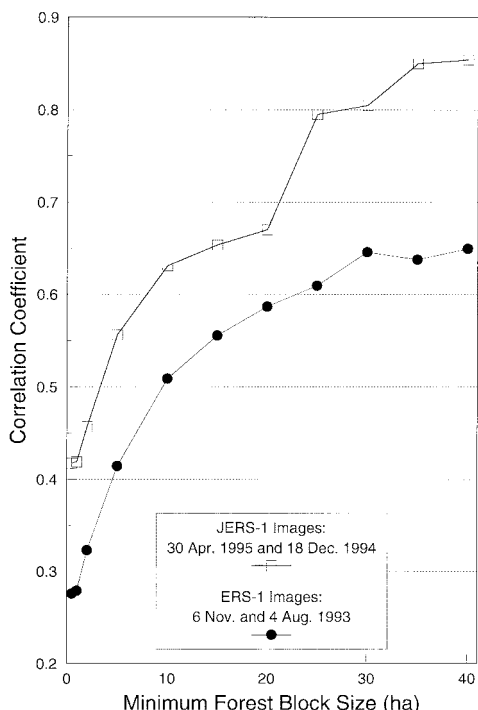


Fig. 5. Correlation between the estimated stem volume and the ground truth versus minimum forest block size. The estimations are based on the JERS-1 image for April 30, 1995, and December 18, 1994, and the ERS-1 image for November 6, 1993, and August 4, 1993. The stem volume estimation is calculated according to (8)–(10).

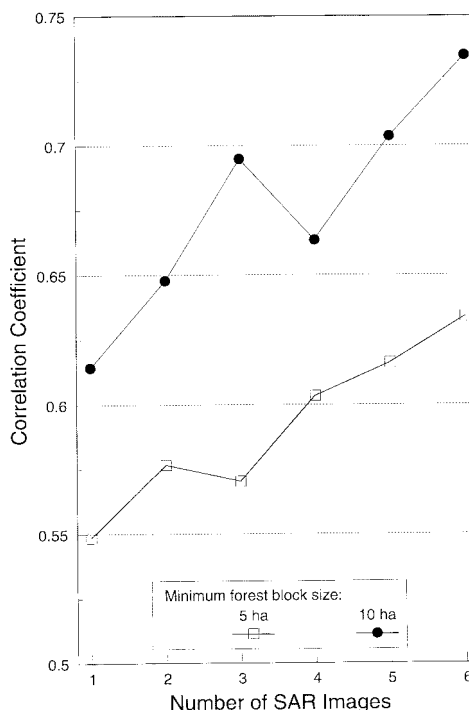


Fig. 7. Correlation between the estimated stem volume and the ground truth versus the number of employed SAR images. Correlation coefficients are presented for forest blocks larger than 5 or 10 ha. One SAR image: JERS-1 for March 15, 1995; Two SAR images: JERS-1 for March 15, 1995, and May 23, 1993; Three SAR images: JERS-1 for March 15, 1995, and May 23, 1993, and ERS-1 for November 6, 1993; Four SAR images: JERS-1 for March 15, 1995, December 18, 1994, and May 23, 1993, and ERS-1 for November 6, 1993; Five SAR images: JERS-1 for March 15, 1995, December 18, 1994, and May 23, 1993, and ERS-1 for August 4, 1993, and November 6, 1993; Six SAR images: JERS-1 for March 15, 1995, December 18, 1994, and May 23, 1993, and ERS-1 for August 4, 1993, October 2, 1993, and November 6, 1993.

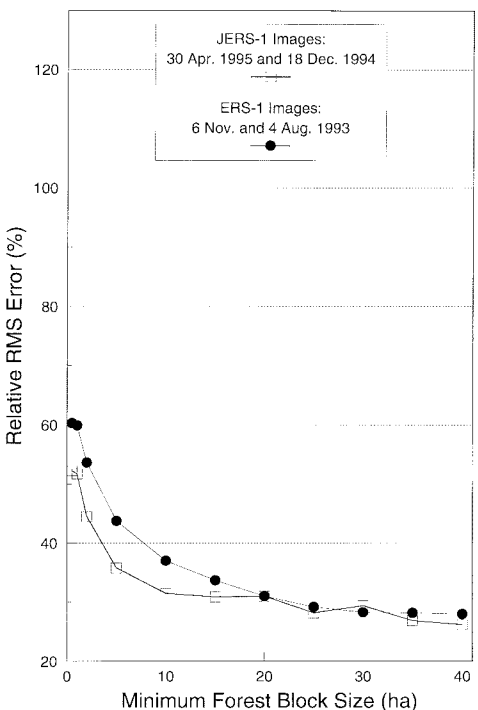


Fig. 6. Relative rms error of the stem volume estimations versus minimum forest block size. The estimations are based on the JERS-1 image for April 30, 1995, and December 18, 1994, and the ERS-1 image for November 6, 1993, and August 4, 1993.

than 5 and 10 ha. Fig. 8 shows the relative rms error of the estimations. The tendency is similar in both cases: when four SAR images were used instead of one, the relative rms error decreased from 43 to 32% for forest blocks that are larger than 5 ha, and from 37 to 27.5% for forest blocks that are larger than 10 ha. The JERS-1 image for March 15, 1995, was used as the single image, and the employed four images were the JERS-1 images for May 23, 1993, December 18, 1994, March 15, 1995, and the ERS-1 image for November 6, 1994. In the six images, ERS-1 images for August 4, 1993, and October 2, 1993, were added to the four images mentioned above; then the relative rms error decreased to 25% and the correlation coefficient was 0.73 for forest blocks that are larger than 10 ha; for forest blocks that are larger than 5 ha, rms error was 31% and correlation coefficient was 0.63.

These results demonstrate that the use of several images reduces 1) the speckle-based error and 2) other random errors in the estimation process. Therefore, the need for spatial averaging is significantly lower. For example, the six images produced 31% relative rms error for forest blocks that were larger than 5 ha, while the rms error for the single image (JERS-1 on March 15, 1995) was still 34% for forest blocks that were larger than 40 ha.

When several SAR images were used, the accuracy of the presented method was at the same level as that of the ground

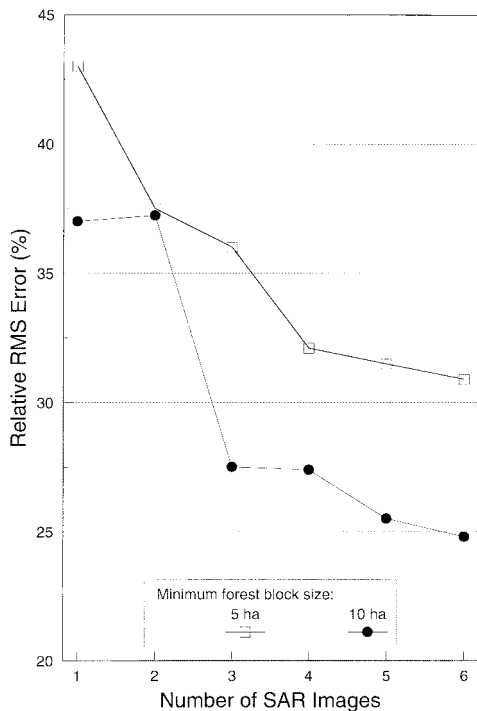


Fig. 8. Relative rms error of the stem volume estimations versus the number of employed SAR images. The rms errors are presented for forest blocks larger than 5 or 10 ha. See the caption of Fig. 7 for the SAR image combinations.

truth (See Section II-A) [26]. The ground truth was used for both training and testing the method. The errors of the ground truth are zero biased and normally distributed. Because the whole training set was applied simultaneously, the ground truth errors did not reduce accuracy of the training. Moreover, it can be expected that the accuracy of the presented results was reduced by uncertainties in the ground truth and the method may exceed the presented reliability levels.

V. CONCLUSIONS

The backscatter levels in *C*-band ERS-1 SAR images were found to be more dependent on weather and seasonal conditions, while that in *L*-band images was less dependent on those factors. Moreover, the *L*-band images were more sensitive to the stem volume than the *C*-band images. At *C*-band, the correlation between the backscattering coefficient and stem volume may change from positive to negative (ERS-1 image for March 13, 1993) depending on weather and seasonal conditions, while at *L*-band, the correlation between the backscattering coefficient and stem volume was always positive. Based on the behavior of the backscattering coefficient discussed above (see Tables II and III), *L*-band (JERS-1) seems more attractive for the biomass estimation than *C*-band. However, the differences in the inversion results are small or nonexistent for large-scale estimation (e.g., areas larger than 20–30 ha; see Figs. 4 and 6).

The inversion algorithm was developed and tested with *L*- and *C*-band SAR images. The inversion method removed successfully the seasonal effects from a single SAR image, and the stem volume inversion was accurate for the large-scale stem volume estimation. These results prove that the

semiempirical model [23] provides an accurate, simple, and useful approximation of the backscattering behavior both at *C*- and *L*-band. In the single image, the estimation of small forest blocks is corrupted by speckle. However, the inversion results were improved significantly for small-scale estimation when several estimations (based on different SAR images) were combined. The relative rms error decreased from 43 to 31% for forest blocks that were larger than 5 ha, when the best single image estimation (JERS-1 image for March 15, 1995) was combined with five other estimations (based on the JERS-1 images for December 18, 1994, and May 23, 1993, and the ERS-1 images for August 4, 1993, October 2, 1993, and November 6, 1993). The JERS-1 images were clearly more feasible for stem volume estimation of the small forest blocks (less than 20–30 ha) than ERS-1 images, but for the large forest blocks (more than 20–30 ha), no difference was found between the JERS-1 or ERS-1 images.

REFERENCES

- [1] J. Pulliainen, P. Mikkilä, M. Hallikainen, and J. P. Ikonen, "Seasonal dynamics of C-band backscattering of boreal forests with application to biomass and soil moisture estimation," *IEEE Trans. Geosci. Remote Sensing*, vol. 34, pp. 758–770, July 1996.
- [2] L. Kurvonen, J. Pulliainen, M. Hallikainen, and P. Mikkilä, "Retrieval of forest parameters from multitemporal spaceborne SAR data," in *Proc. IGARSS'96 Symp.*, Lincoln, NE, pp. 1759–1762.
- [3] L. Kurvonen, J. Pulliainen, and M. Hallikainen, "Monitoring of boreal forests with multitemporal SSM/I data," *Radio Sci.*, vol. 33, pp. 731–744, May–June 1998.
- [4] L. Kurvonen and M. Hallikainen, "Textural information of multitemporal ERS-1 and JERS-1 SAR images with applications to land and forest type recognition in boreal zone," *IEEE Trans. Geosci. Remote Sensing*, to be published.
- [5] M. Dobson, F. Ulaby, T. Le Toan, A. Beaudoin, E. Kasischke, and N. Christensen, "Dependence of radar backscatter on coniferous forest biomass," *IEEE Trans. Geosci. Remote Sensing*, vol. 30, pp. 412–414, Mar. 1992.
- [6] E. Kasischke, N. Christensen, L. Bourgeau-Chavez, and E. Haney, "Observations on the sensitivity of ERS-1 SAR image intensity to changes in above ground biomass in young loblolly pine forests," *Int. J. Remote Sensing*, vol. 15, pp. 3–16, 1994.
- [7] J. Rauste, T. Häme, J. Pulliainen, K. Heiska, and M. Hallikainen, "Radar-based forest biomass estimation," *Int. J. Remote Sensing*, vol. 15, no. 14, pp. 2797–2808, 1994.
- [8] E. Rignot, J. Way, C. Williams, L. Viereck, J. Yarie, and T. Le Toan, "Radar estimates of above ground biomass in boreal forests of interior Alaska," *IEEE Trans. Geosci. Remote Sensing*, vol. 32, pp. 1117–1124, Sept. 1994.
- [9] T. Le Toan, A. Beaudoin, J. Riom, and D. Guyon, "Relating forest biomass to SAR data," *IEEE Trans. Geosci. Remote Sensing*, vol. 30, pp. 403–411, Mar. 1992.
- [10] J. Pulliainen, K. Heiska, J. Hyypä, and M. Hallikainen, "Backscattering properties of boreal forests at the C- and X-bands," *IEEE Trans. Geosci. Remote Sensing*, vol. 32, pp. 1041–1050, Nov. 1994.
- [11] Y. Dong and J. Richards, "Multifrequency radar analysis of forests," Final Rep. JERS-1/ERS-1 Syst. Verification Program, MITI/NASDA, 1995, vol. II, pp. 9–17.
- [12] H. Israelsson, J. Askne, J. Fransson, and R. Sylvander, "JERS-1 SAR analysis of boreal forest biomass," Final Rep. JERS-1/ERS-1 Syst. Verification Program, MITI/NASDA, 1995, vol. II, pp. 38–45.
- [13] M. Dobson, L. Pierce, K. McDonald, and T. Sharik, "Seasonal change in radar backscatter from mixed conifer and hardwood forests in northern Michigan," in *Proc. IGARSS'91 Symp.*, Espoo, Finland, pp. 1121–1124.
- [14] F. Ahern, D. Leckie, and J. Drieman, "Seasonal changes in relative C-band backscatter of northern forest cover types," *IEEE Trans. Geosci. Remote Sensing*, vol. 31, pp. 668–680, July 1993.
- [15] E. Rignot, K. McDonald, L. Viereck, and P. Adams, "Monitoring of environmental conditions in the Alaskan forests using ERS-1 data," in *Proc. IGARSS'92 Symp.*, Houston, TX, pp. 530–532.
- [16] E. Rignot, J. B. Way, K. McDonald, L. Viereck, C. Williams, P. Adams, C. Payne, W. Wood, and J. Shi, "Monitoring of environmental conditions

- in taiga forests using ERS-1 SAR," *Remote Sens. Environ.*, vol. 49, pp. 145–154, 1994.
- [17] J. B. Way, E. Rignot, K. McDonald, R. Oren, R. Kwok, G. Bonan, M. Dobson, L. Viereck, and J. Roth, "Evaluating the type and state of Alaska taiga forests with imaging radar for use in ecosystem models," *IEEE Trans. Geosci. Remote Sensing*, vol. 32, pp. 353–370, Mar. 1994.
- [18] T. Häme, A. Salli, and K. Lahti, "Estimation of carbon storage in boreal forests using remote sensing data," in *The Finnish Research Programme on Climate Change, Progress Report*, K. Kanninen and P. Anttila, Eds. Helsinki, Finland: Acad. Finland, 1992, pp. 250–252.
- [19] Finnish Forest Research Institute, "The 8th National Forest Inventory: Instructions for field work," Dept. Forest Inventory, Finnish Forest Res. Inst., Helsinki, Finland, 1988.
- [20] European Space Agency, "ERS-1 User Handbook," Eur. Space Agency (ESA), ESA Publ. Division, Noordwijk, The Netherlands, ESA SP-1148, 1992.
- [21] National Space Development Agency of Japan, "JERS-1 Data Users Handbook," Nat. Space Development Agency of Japan (NASDA), Earth Observation Center, Saitama-ken, Japan, 1994.
- [22] J. Pulliainen, *Investigation on the Backscattering Properties of Finnish Boreal Forests at C- and X-Band: A Semi-Empirical Modeling Approach*, Ph.D. dissertation, Lab. Space Technol., Helsinki Univ. Technol., Espoo, Finland, Rep. 19, 1994.
- [23] M. Hallikainen *et al.*, "A helicopter-borne eight-channel ranging scatterometer for remote sensing—Part I: System description," *IEEE Trans. Geosci. Remote Sensing*, vol. 31, pp. 161–169, Jan. 1993.
- [24] E. Attema and F. Ulaby, "Vegetation modeled as a water cloud," *Radio Sci.*, vol. 13, no. 2, pp. 357–364.
- [25] Y. Rauste, "Methods for analyzing SAR images," Lab. Instrumentation Technol., Tech. Res. Centre Finland, Espoo, 1989, Rep. 612.
- [26] E. Tomppo, "Recent status and further development of the Finnish multi-source forest inventory," in *Proc. 1997 Marcus Wallenberg Prize Symp.*, Stockholm, Sweden, pp. 53–70; ISSN 0282–4647.



Lauri Kurvonen was born on October 14, 1964, in Orimatilla, Finland. He received the M.Sc., the Licentiate, and the Doctor of Technology degrees in electrical engineering from Helsinki University of Technology (HUT), Espoo, Finland.

He was a Research Fellow at the Space Applications Institute, Joint Research Centre of European Commission, Ispra, Italy, from 1995 to 1997. Presently, he is a Research Scientist at the Space Laboratory, HUT, and a Principal Lecturer of space and aviation technologies at Rovaniemi Institute

of Technology, Finland. His research interests include active and passive microwave remote sensing of ice, snow, and forest.

Jouni Pulliainen received the M.Sc., the Licentiate, and the Doctor of Technology degrees from the Helsinki University of Technology (HUT), Espoo, Finland, in 1988, 1991, and 1994, respectively.

He was Acting Director of the Laboratory of Space Technology, HUT, from 1993 to 1994. He has been a Docent of Space Technology at HUT since 1997, specializing in remote sensing. He is currently a Research Scientist in the Laboratory of Space Technology, HUT. His research interests include microwave remote-sensing applications and technology. Recently, his work has focused on the active and passive remote sensing of boreal forest zone and snow cover. He has directed several remote-sensing research projects in the Laboratory of Space Technology. He has authored over 90 scientific papers and reports in the field of remote sensing.



Martti Hallikainen (M'83–SM'85–F'93) received the M.Sc. degree in engineering and the Doctor of Technology degree from the Helsinki University of Technology (HUT), Espoo, Finland, in 1971 and 1980, respectively.

He was a Visiting Scientist in 1993–1994 at the European Union's Joint Research Centre, Institute for Remote Sensing Applications, Ispra, Italy. He was a Postdoctoral Fellow at the Remote Sensing Laboratory, University of Kansas, Lawrence, from 1981 to 1983. Since 1987, he has been a Professor of Space Technology at the Helsinki University of Technology, where his research interests include remote sensing and satellite technology. He established the HUT Laboratory of Space Technology in 1988 and serves as its Director.

Dr. Hallikainen was President of the IEEE Geoscience and Remote Sensing Society (IEEE/GRSS) in 1996 and 1997 and Vice President in 1994 and 1995. Since 1988, he has been a member of the IEEE GRSS Administrative Committee. He was General Chairman of the IGARSS'91 Symposium and Guest Editor of the Special IGARSS'91 Issue of the IEEE TRANSACTIONS ON GEOSCIENCE AND REMOTE SENSING (TGARS). Since 1992, he has been an Associate Editor of TGARS. He was a member of the IEEE Periodicals Committee in 1997 and a Corresponding Member of the IEEE New Technology Directions Committee in 1992–1995. He was Secretary General of the European Association of Remote Sensing Laboratories (EARSeL) in 1989–1993 and Chairman of the Organizing Committee for the EARSeL 1989 General Assembly and Symposium. He has been a member of the EARSeL Council since 1985, and he was a member of the Editorial Board of the EARSeL Advances in Remote Sensing in 1992–1993. He was a National Delegate to the European Space Agency (ESA) Earth Observation Scientific and Technical Advisory Group (EOSTAG) in 1988–1994, and he has served in the same capacity on the ESA Earth Observation Data Operations Scientific and Technical Advisory Group (DOSTAG) since 1995. He also presently serves on the ESA Earth Sciences Advisory Committee (ESAC). He was Thematic Coordinator of ESA EMAC-95 airborne campaign for snow and ice activities. He was a member of the ESA Multi-Frequency Imaging Microwave Radiometer (MIMR) Expert Group in 1988–1994 and a member of the ESA MIMR Scientific Advisory Group in 1994–1996. He has been a member of the Advisory Committee for the European Microwave Signature Laboratory of the European Union's Joint Research Centre since 1992 and International Space University National Liaison since 1992. He has been a member of the URSI Long Range Planning Committee since 1996, an official member of the URSI Commission F (Wave Propagation and Remote Sensing) since 1988, and a member of the URSI Committee on Geosphere and Biosphere Program since 1989. He was Secretary of the Organizing Committee for the URSI Nordic Antenna Symposium in 1976, and he served as Secretary of the Finnish National Committee of URSI from 1975 to 1989. He was Vice Chairman of the URSI Finnish National Committee from 1990 to 1996, and he has served as the Chairman since 1997. He was the recipient of the IEEE IGARSS'96 Interactive Paper Award and the IEEE GRSS 1994 Outstanding Service Award. He is a winner of the Microwave Prize for the best paper in the 1992 European Microwave Conference, and he received the HUT Foundation Award for excellence in research in 1990. He and his research team received the 1989 National Research Project of the Year Award from Tekniikka & Talous (*Technology & Management Magazine*). He received the 1984 Sähkö–Electricity in Finland Editorial Board Prize. He was awarded an ASLA Fulbright Scholarship with the University of Texas at Austin in 1974–1975.